RMetS
Royal Meteorological Society

Revisiting the formulations for the longitudinal velocity variance in the unstable atmospheric surface layer

T. Banerjee,[a*] G. G. Katul,[a,b] S. T. Salesky[c] and M. Chamecki[c]
[a]*Nicholas School of the Environment, Duke University, Durham, NC, USA*
[b]*Department of Civil and Environmental Engineering, Duke University, Durham, NC, USA*
[c]*Department of Meteorology, The Pennsylvania State University, University Park, PA, USA*

*Correspondence to: T. Banerjee, Nicholas School of the Environment, Duke University, Box 90328, Durham, NC 27708, USA.
E-mail: tirtha.b@duke.edu

Because of its non-conformity to Monin–Obukhov Similarity Theory (MOST), the effects of thermal stratification on scaling laws describing the streamwise turbulent intensity σ_u normalized by the turbulent friction velocity (u_*) continue to draw research attention. A spectral budget method has been developed to assess the variability of σ_u/u_* under unstable atmospheric stratification. At least three different length-scales – the distance from the ground (z), the height of the atmospheric boundary layer (δ) and the Obukhov length (L)–are all found to be controlling parameters in the variation of σ_u/u_*. Analytical models have been developed and supported by experiments for two limiting conditions: $z/\delta < 0.02$, $-z/L < 0.5$ and $0.02 \ll z/\delta < 0.1$, $-z/L > 0.5$. Under the first constraint, the turbulent kinetic energy spectrum is predicted to follow three regimes: k^0, k^{-1} and $k^{-5/3}$, divided in the last two regimes by a break-point at $kz = 1$, where k denotes the wave number. The quantity σ_u/u_* is shown to follow the much discussed logarithmic scaling, reconciled to Townsend's attached eddy hypothesis $\sigma_u^2/u_*^2 = B_1 - A_1 \log(z/\delta)$, where the coefficients B_1 and A_1 are modified by MOST for mildly unstable stratification. Under the second constraint, the turbulent energy spectrum tends to become quasi-inertial, displaying k^0 and $k^{-5/3}$ with a break-point predicted to occur at $0.3 < kz < 1$. The work here brings together well-established but seemingly unrelated theories of turbulence such as Kolmogorov's hypothesis, Townsend's attached eddy hypothesis, MOST and Heisenberg's eddy viscosity under a common framework.

Key Words: Heisenberg's eddy viscosity; logarithmic scaling; Monin–Obukhov similarity theory; spectral budget; streamwise turbulent intensity; Townsend's attached eddy hypothesis

Received 10 March 2014; Revised 5 August 2014; Accepted 20 September 2014; Published online in Wiley Online Library

1. Introduction

Scaling laws of the root-mean-squared longitudinal turbulent velocity component (σ_u) with distance from a solid boundary (z) in high-Reynolds-number turbulent flows are receiving renewed interest (Alfredsson *et al.*, 2011; Smits and Marusic, 2013), given their relevance to a myriad of meteorological problems regarding wind-power generation, dispersion of pollutants and footprint estimation among others (Poggi *et al.*, 2006; Cai *et al.*, 2008; Hsieh and Katul, 2009; Hansen *et al.*, 2012; McKeon, 2013; Yang *et al.*, 2014). A logarithmic scaling of the form $\sigma_u^2/u_*^2 = B_1 - A_1 \log(z/\delta)$ has been proposed by Townsend (1976), where u_* is the friction velocity, A_1, B_1 are constants and δ is the boundary-layer height. Recent laboratory experiments confirmed the universal character of a log-law scaling in σ_u/u_* within a region where the normalized mean velocity profile also exhibits a log-law scaling (Marusic *et al.*, 2013; McKeon, 2013; Smits and Marusic, 2013), expressed as $U/u_* = \kappa^{-1}\log(z) + C_w$, where κ is the von Kármán constant and C_w is a surface roughness coefficient.

In the atmospheric surface layer (ASL), distortions to the U/u_* log law due to the presence of thermal stratification can be accommodated using Monin–Obukhov similarity theory (MOST) via a stability correction function that varies with the atmospheric stability parameter $\zeta = z/L$, where L is the Obukhov length (Obukhov, 1946; Monin and Obukhov, 1954). Recent theoretical and phenomenological arguments suggest that the stability correction function to U/u_* appears to inherit its quasi-universal character from the shape of the turbulent spectrum (Katul *et al.*, 2011, 2013a) and the variations of the integral length-scale of the flow with atmospheric stability (Salesky *et al.*, 2013).

However, the effects of thermal stratification on σ_u/u_* remain a thorny issue within the MOST framework. The earliest attempts identified acceptable scaling with ζ for vertical turbulent intensity σ_w/u_*, but mixed success with σ_u/u_* was already noted (Lumley

and Panofsky, 1964). Panofsky *et al.* (1977) even precluded the possibility of a ζ scaling and proposed a $(\delta/L)^{1/3}$ power-law scaling for σ_u/u_* for unstable stratification. The lack of a universal similarity behaviour of σ_u/u_* was also discussed by Townsend (1961) and supported by Bradshaw (1967), Bradshaw (1978), Kaimal (1978) and Yaglom (1994). While the Panofsky *et al.* (1977) scaling has been used (Liu *et al.*, 2011) and included in standard micro-meteorology literature (Sorbjan, 1989; Kaimal and Finnigan, 1994), other experiments did report a 1/3 scaling with ζ for σ_u/u_*, especially for tower measurements close to the ground (Hicks, 1981; Hsieh and Katul, 1997). Further, a modification was suggested by Wilson (2008), who appended a multiplicative z/δ dependence to Panofsky's scaling (Panofsky *et al.*, 1977), similar to Rodean (1996), which is constrained by the condition $z \ll \delta$.

The goal of this work is to explain the onset of these divergent results for σ_u/u_* under a common framework, using a turbulent kinetic energy spectral budget. It has been shown elsewhere (Banerjee and Katul, 2013) that a spectral budget method (Hinze, 1959; Panchev, 1971) can recover the logarithmic scaling in σ_u^2/u_*^2 in the absence of thermal stratification and provide a theoretical basis for linking A_1 and B_1 to the Kolmogorov constant describing the turbulent kinetic energy spectrum within the inertial subrange. This spectral budget is expanded here to include the effects of thermal stratification explicitly using a new source term attributed to the presence of a finite sensible heat flux. The main theoretical contribution is an analytical expression linking σ_u^2/u_*^2 to both ζ and z/δ, at least when $|\zeta|$ is small (<0.5) and varies primarily due to variations in land-surface fluxes (i.e. L).

The newly derived expression can be further simplified to show under what conditions A_1 and B_1 actually vary with ζ, thereby generalizing Townsend's attached eddy hypothesis for neutral flows to mildly unstable ASL via MOST. For large z variations, other considerations must be accommodated in the spectral budget that preclude a complete solution. However, under some restrictive assumptions, the scaling proposed by Panofsky and its variant (Wilson, 2008) may be recovered.

Before considering the behaviour of σ_u/u_* for such unstably stratified flow, the model prediction in the near-neutral stability limit ($\zeta \to 0$) is briefly reviewed and compared with results from recent laboratory experiments. The large scatter in the near-neutral σ_u/u_* value reported in several ASL studies, often varying between 2 and 3 (McBean, 1971; Panofsky *et al.*, 1977; Panofsky and Dutton, 1984; Kader and Yaglom, 1990; Hsieh and Katul, 1997; Pahlow *et al.*, 2001; Liu *et al.*, 2011), is shown to be explicitly related to differences in δ across experiments and can be explained by Townsend's hypothesis. A recent dataset is also employed to explore assumptions and provide support for the proposed analysis. As will be seen, the present analysis provides a basis for bridging different concepts such as Townsend's attached eddy hypothesis, the k^{-1} and $k^{-5/3}$ spectral laws at low wave numbers and the similarity arguments for an unstably stratified ASL.

2. Theory

2.1. Background and definitions

In the ASL, the time-averaged longitudinal momentum balance and heat budget equations are given by

$$\frac{\partial U}{\partial t} + U_j \frac{\partial U}{\partial x_j} = \nu \frac{\partial^2 U}{\partial x_j \partial x_j} - \frac{\partial \overline{u' u_j'}}{\partial x_j} - \frac{1}{\rho}\frac{\partial P}{\partial x}, \tag{1}$$

$$\frac{\partial T}{\partial t} + U_j \frac{\partial T}{\partial x_j} = D_\mathrm{m} \frac{\partial^2 T}{\partial x_j \partial x_j} - \frac{\partial \overline{u_j' T'}}{\partial x_j}, \tag{2}$$

where t is time, U_j are the time-averaged velocity components along direction x_j and $x_j = (x, y, z)$ are the longitudinal ($= x$), lateral ($= y$) and vertical ($= z$) directions, with the longitudinal direction aligned so that $U_2 = 0$. Here, U (or U_1), T and P represent the time-averaged longitudinal velocity, temperature and pressure, respectively, ρ is the mean air density, ν is the mean air kinematic viscosity, D_m is the molecular diffusivity of heat in air, $u_i' = (u', v', w')$ are the component-wise turbulent velocity excursions in direction x_i, T' is the turbulent temperature fluctuation and, unless otherwise stated, primed quantities represent turbulent excursions from the time-averaged state represented by overbar or capital letter symbols. Hence, the instantaneous velocity and temperature can be expressed as $U_i + u_i'$ and $T + T'$, respectively. For an idealized ASL, the flow can be simplified so that it can satisfy the following conditions:

1. high Reynolds and Peclet numbers (i.e. neglect molecular viscosity and diffusivity relative to their turbulent counterparts in the mean momentum and heat budget equations);
2. stationary (i.e. $\partial(\cdot)/\partial t = 0$) and planar-homogeneous (i.e. $\partial(\cdot)/\partial x = \partial(\cdot)/\partial y = 0$); and
3. lack of any subsidence (i.e. $U_3 = W = 0$) or significant mean horizontal pressure gradients (i.e. $\partial P/\partial x = 0$).

For these idealized conditions, the mean longitudinal momentum balance and the mean heat budget equations in the ASL reduce to $\partial \overline{w'u'}/\partial z = 0$ and $\partial \overline{w'T'}/\partial z = 0$, suggesting that the turbulent stress (i.e. $\overline{w'u'}$) and heat flux (i.e. $\overline{w'T'}$) are constant with z. It is for this reason that the ASL subjected to such idealized assumptions is labelled as the constant-stress or constant-flux layer (Brutsaert, 1982).

The time-averaged turbulent kinetic energy (TKE) budget in this idealized ASL is

$$\frac{\partial e}{\partial t} = 0 = -\overline{u'w'}\frac{\mathrm{d}\bar{U}}{\mathrm{d}z} + \frac{g}{T}\overline{w'T'} - \frac{\partial}{\partial z}\left(\frac{1}{2}\overline{w'\left(u'^2 + v'^2 + w'^2\right)} + \frac{1}{\rho}\overline{w'p'}\right) - \bar{\epsilon}, \tag{3}$$

where $e = (1/2)\left(\sigma_u^2 + \sigma_v^2 + \sigma_w^2\right)$ is the TKE, $\sigma_u^2 = \overline{u'^2}$, $\sigma_v^2 = \overline{v'^2}$ and $\sigma_w^2 = \overline{w'^2}$. The first, second, third and fourth terms on the right-hand side (RHS) of Eq. (3) are, respectively, the mechanical and buoyant production (or dissipation) of TKE, the TKE transport by turbulence and pressure–velocity interactions and the viscous dissipation of TKE. In the ASL, the transport terms have opposite signs, often producing small net TKE transport and a near-balance between production and dissipation of TKE, even though some studies report a significant imbalance. The sign and magnitude of this imbalance remains uncertain and will be neglected here. However, it is to be noted that unstable cases often report superior balance between TKE production and dissipation compared with stable cases (Townsend, 1976; Pope, 2000; Charuchittipan and Wilson, 2009). As evident from Eq. (3), when $\overline{w'T'} > 0$ (e.g. during daytime conditions over land), the second term is a source of TKE and the ASL flow is labelled as unstable. Near-neutral conditions prevail when $\overline{w'T'} = 0$ and stable conditions occur when $\overline{w'T'} < 0$ (e.g. nocturnal conditions over land). For the mean states, MOST (Monin and Obukhov, 1954) yields $\mathrm{d}\bar{U}/\mathrm{d}z = \phi_\mathrm{m}(\zeta)\, u_*/(\kappa z)$ and $\bar{\epsilon} = (\phi_\mathrm{m}(\zeta) - (\zeta))\, u_*^3/(\kappa z)$, where $L = -{u_*}^3/(\kappa\, (g/T)\, \overline{w'T'})$, g is gravitational acceleration and $\phi_\mathrm{m}(\zeta)$ is the stability correction function for momentum. The function $\phi_\mathrm{m}(\zeta)$ can be described by the widely used empirical Businger–Dyer (Businger and Yaglom, 1971; Dyer, 1974) form $\phi_\mathrm{m}(\zeta) = (1 - 16\zeta)^{-1/4}$ for $\zeta < 0$ (i.e. unstable conditions), which constitutes the stability conditions explored here.

2.2. A spectral budget

If $\bar{\epsilon}$ is a conservative quantity across the turbulent energy cascade (i.e. total TKE production is balanced by TKE transfer across

all wave numbers within the inertial subrange and is further balanced by TKE removal through viscous dissipation at large wave numbers), then a simplified spectral budget can be derived for any wave number k, given as (Hinze, 1959; Panchev, 1971)

$$\bar{\epsilon} = -\frac{\mathrm{d}\bar{U}}{\mathrm{d}z}\int_k^\infty F_{wu}(s)\,\mathrm{d}s + \frac{g}{T}\int_k^\infty F_{wT}(s)\,\mathrm{d}s + F(k) + 2\nu\int_0^k s^2 E_{\mathrm{tke}}(s)\,\mathrm{d}s, \quad (4)$$

where the first, second, third and fourth terms on the RHS represent, as before, the mechanical and buoyant production of TKE in the range [k, ∞], the transfer of TKE in the range [k, ∞] and the viscous dissipation in the range $[0, k]$. Two conditions are imposed on $F(k)$ so as to ensure that this spectral budget recovers its time-averaged TKE counterpart in Eq. (3) when spectrally integrated across all k. The first condition is that at $k = 0$, $F(0) = 0$ and

$$\bar{\epsilon} = -\frac{\mathrm{d}\overline{U}}{\mathrm{d}z}\int_0^\infty F_{wu}(s)\,\mathrm{d}s + \frac{g}{T}\int_0^\infty F_{wT}(s)\,\mathrm{d}s = -\frac{\mathrm{d}\bar{U}}{\mathrm{d}z}\left(\overline{u'w'}\right) + \frac{g}{T}\,\overline{w'T'}, \quad (5)$$

so that $\int_0^\infty F_{wu}(s)\,\mathrm{d}s = \overline{u'w'}$ and $\int_0^\infty F_{wT}(s)\,\mathrm{d}s = \overline{w'T'}$ maintain the balance between production (mechanical and buoyant) and $\bar{\epsilon}$.

The second condition is that as $k \to \infty$, $F(\infty) \to 0$ and

$$\bar{\epsilon} \approx 2\nu\int_0^\infty s^2 E_{\mathrm{tke}}(s)\,\mathrm{d}s, \quad (6)$$

or $\bar{\epsilon}$ is primarily explained by viscous contributions at very large k. The transfer of turbulent kinetic energy $F(k)$ across wave number k is related to the action of the triple moments and the pressure–velocity interaction (i.e $\int_0^\infty F(k)\,\mathrm{d}k = (1/2)\partial(\overline{w'\left(u'^2+v'^2+w'^2\right)})/\partial z + \rho^{-1}\partial(\overline{w'p'})/\partial z$, the two transport terms in the TKE budget) and requires closure. The Heisenberg model (Heisenberg, 1948) can be employed to achieve such a closure and is given by

$$F(k) = \nu_t(k)\overline{|\mathrm{curl}\,\tilde{u}|^2} \approx 2\nu_t(k)\int_0^k s^2 E_{\mathrm{tke}}(s)\,\mathrm{d}s, \quad (7)$$

where $\tilde{u}$ is a 'macro-scale' component of the velocity and $\nu_t(k)$ is the so-called Heisenberg eddy viscosity (Heisenberg, 1948). It is produced by the motion of eddies with wave numbers exceeding k and is given by

$$\nu_t(k) = C_{\mathrm{H}}\int_k^\infty \sqrt{\frac{E_{\mathrm{tke}}(s)}{s^3}}\,\mathrm{d}s, \quad (8)$$

where C_{H} is the Heisenberg constant to be discussed later. With these approximations and closure assumptions, the spectral budget for the TKE in the ASL reduces to

$$\bar{\epsilon} = -\frac{\mathrm{d}\bar{U}}{\mathrm{d}z}\int_k^\infty F_{wu}(s)\,\mathrm{d}s + 2\left(\nu_t(k)+\nu\right)\int_0^k s^2 E_{\mathrm{tke}}(s)\,\mathrm{d}s + \frac{g}{T}\int_k^\infty F_{wT}(s)\,\mathrm{d}s. \quad (9)$$

2.3. *The spectral budget at k_a=1/z*

While valid for all k, Eq. (9) is now evaluated at a specific $k_{\mathrm{a}} = 1/z$ within the ASL. It is assumed that, for $kz > 1$ (i.e. small scales), $E_{\mathrm{tke}}(k)$ and $F_{wu}(k)$ are described by their conventional (Kolmogorov, 1941) and (Lumley, 1967) scaling forms, respectively, given as

$$E_{\mathrm{tke}}(k) = C_{\mathrm{o}}\overline{\epsilon}^{2/3}k^{-5/3}, \quad (10)$$

and

$$F_{wu}(k) = -\frac{\mathrm{d}\bar{U}}{\mathrm{d}z}C_{uw}\overline{\epsilon}^{1/3}k^{-7/3}, \quad (11)$$

where C_{o} is the Kolmogorov constant and C_{uw} is a similarity constant (Saddoughi and Veeravalli, 1994; Pope, 2000; Ishihara *et al.*, 2002; Katul *et al.*, 2013b). Using these spectral and co-spectral scaling expressions for $k > 1/z$,

$$\frac{\mathrm{d}\bar{U}}{\mathrm{d}z}\int_{k_{\mathrm{a}}}^\infty F_{wu}(s)\,\mathrm{d}s = -\frac{3}{4}\left(\frac{\mathrm{d}\bar{U}}{\mathrm{d}z}\right)^2 C_{uw}\overline{\epsilon}^{1/3}k_{\mathrm{a}}^{-4/3}, \quad (12)$$

and

$$\nu_t(k_{\mathrm{a}}) = C_{\mathrm{H}}\int_{k_{\mathrm{a}}}^\infty \sqrt{\frac{C_{\mathrm{o}}\overline{\epsilon}^{2/3}s^{-5/3}}{s^3}}\,\mathrm{d}s = \frac{3C_{\mathrm{H}}C_{\mathrm{o}}^{1/2}\overline{\epsilon}^{1/3}}{4k_{\mathrm{a}}^{4/3}}. \quad (13)$$

With the Kolmogorov microscale defined as $\eta = (\nu^3/\overline{\epsilon})^{1/4}$, it is interesting to note that the ratio of turbulent to molecular viscosity at $k = k_{\mathrm{a}} = 1/z$ is given by

$$\frac{\nu_t(k_{\mathrm{a}})}{\nu} = \frac{3C_{\mathrm{H}}C_{\mathrm{o}}^{1/2}}{4(k_{\mathrm{a}}\eta)^{4/3}}. \quad (14)$$

Because $k_{\mathrm{a}}\eta \ll 1$ in the ASL, $\nu \ll \nu_t(k_{\mathrm{a}})$ and $\nu + \nu_t \approx \nu_t$ in Eq. (9).

To evaluate the buoyancy production for $k_{\mathrm{a}} \le k < \infty$, the co-spectral scaling for $F_{wT}(k)$ is used; this is given by Kader and Yaglom (1991); Kaimal and Finnigan (1994); Cava and Katul (2012); Katul *et al.* (2013a)

$$F_{wT} = C'_{wT}\frac{\mathrm{d}T}{\mathrm{d}z}\,\bar{\epsilon}^{1/3}\,k^{-7/3}, \quad (15)$$

where

$$C'_{wT} = \left(1 - \frac{3}{2}\frac{(4/3)\,C_T}{C_{\mathrm{o}}}\frac{\zeta}{\phi_{\mathrm{m}}(\zeta)-\zeta}\right)C_{wT}, \quad (16)$$

and where $C_T = 0.8$ is known as the Kolmogorov–Obukhov–Corrsin constant (Corrsin, 1951), C_{wT} is a co-spectral similarity constant (Kaimal and Finnigan, 1994; Katul *et al.*, 2013a, 2014) and $T_* = -\overline{w'T'}/u_*$ is the ASL temperature scale. The derivation of Eq. (15) assumes that production and dissipation terms in the temperature variance budget are also in balance (Katul *et al.*, 2013a). It is hereby noted that, using the definition of L, T_* can be written as

$$T_* = \frac{u_*^2}{\kappa\,(g/T)\,L}. \quad (17)$$

Also, MOST scaling for the mean temperature profile results in

$$\frac{\mathrm{d}T}{\mathrm{d}z} = \frac{T_*}{\kappa\,z}\,\phi_T(\zeta), \quad (18)$$

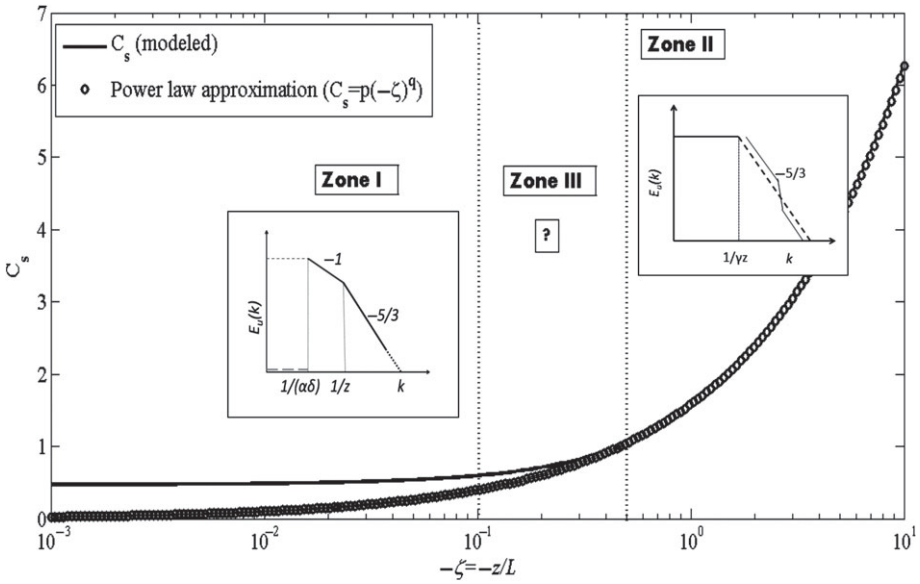

Figure 1. The modelled $C_s(\zeta)$ according to Eq. (21) and fitted with a power law of the form $C_s = p\,(\zeta)^q$, where $p = 1.6$ and $q = 0.6$. It is found that the power law is a good fit for $C_s(\zeta)$ after $-\zeta = 0.5$, represented by a dotted line (labelled as Zone II). A constant C_s appears to be reasonable for $-\zeta < 0.5$ (labelled as Zone I).

where $\phi_T(\zeta)$ is the stability correction function for heat, which can be described by the Businger–Dyer equation as $\phi_T(\zeta) = \phi_m(\zeta)^2$ in unstable conditions (Dyer, 1974). Justification beyond dimensional considerations for $\phi_T(\zeta) = \phi_m(\zeta)^2$ is reviewed elsewhere (Li *et al.*, 2012) and is not repeated here.

Using the definition of $F_{wT}(k)$, the buoyancy production contribution can be determined as

$$\frac{g}{T}\int_{k_a}^{\infty} F_{wT}(s)\,\mathrm{d}s = \frac{3}{4}\,\frac{g}{T}\,\frac{T_*}{\kappa\, z}\,\phi_T(\zeta)\,C'_{wT}\,\bar{\epsilon}^{1/3}\,{k_a}^{-4/3}. \tag{19}$$

Again, in the ASL, $\mathrm{d}\bar{U}/\mathrm{d}z = \phi_m(\zeta)\,u_*/(\kappa z)$, $\bar{\epsilon} = (\phi_m(\zeta) - \zeta)\,u_*^3/(\kappa z)$ and, using $F_{wu}(k)$ from Eqs (11) and (19) along with Eqs (17) and (9), simplifies to

$$\int_0^{k_a} s^2 E_{tke}(s)\,\mathrm{d}s = \frac{u_*^2}{z^2} C_s, \tag{20}$$

where $C_s(\zeta)$ varies with ζ and is given by

$$C_s = \frac{2}{3C_H C_o^{1/2}}\left((\phi_m(\zeta) - \zeta)^{2/3}\kappa^{4/3}/\kappa^2 - (3/4)\,C_{uw}\,\phi_m(\zeta)^2/\kappa^2 - (3/4)\,\zeta\,C'_{wT}\,\phi_T(\zeta)/\kappa^2\right). \tag{21}$$

Any formulation for $E_{tke}(k)$ requires an analytical expression for C_s. To estimate C_s, standard values for the constants $\kappa = 0.4$, $C_o = 0.55$, $C_{uw} = 0.15$ and $C_H = (8/9)\,C_o^{-3/2}$ as derived for isotropic conditions (Schumann, 1994) are used. The other constant C_{wT} is taken as (Kaimal and Finnigan, 1994) $C_{wT} = 3\,C_{uw}$. By this particular choice of constants for C_o, C_H and C_{uw}, the issue of projecting the three-dimensional transport term to a one-dimensional wave-number form has been bypassed (Ishihara *et al.*, 2002). The variation of C_s with ζ is shown in Figure 1 and the discussion on $E_{tke}(k)$ is now based on how C_s varies with atmospheric stability. It is evident from Figure 1 that, for $|\zeta| < 0.1$ (labelled as Zone I), C_s is approximately constant. Also, for $|\zeta| > 0.5$ (labelled as Zone II), C_s is well represented by an approximate power law of the form $C_s = p\,(\zeta)^q$. When this power-law form is fitted to the expression for $C_s(\zeta)$ given by Eq. (21) and for $|\zeta| > 0.5$, an acceptable statistical fit is achieved when $p = 1.6$ and $q = 0.6$, with a coefficient of determination $R^2 > 0.99$. For these two zones describing C_s variation with ζ, it is possible to derive explicit analytical expressions for $E_{tke}(k)$ and track the consequences of these expressions for σ_u/u_*.

2.4. *Formulation for Zone I*

To solve for $E_{tke}(k)$ in Eq. (20) for $kz \le 1$, a power-law solution with undetermined coefficients is first assumed, so that $E_{tke}(k) = a_1 k^{b_1}$. This assumed power-law solution is then inserted into Eq. (20) to yield

$$\frac{a_1 z^{-3-b_1}}{3 + b_1} = \frac{u_*^2}{z^2} C_s, \tag{22}$$

where C_s is approximately a constant independent of z in Zone I. A plausible polynomial matching between the left- and right-hand sides yields $-3 - b_1 = -2$ or $b_1 = -1$ and $a_1 = 2C_s u_*^2$. This analysis suggests that $E_{tke}(k) = C'_{TKE} u_*^2 k^{-1}$, thereby recovering the -1 power law in the spectrum of TKE (Tchen, 1953; Panchev, 1971; Perry and Abell, 1977; Turan *et al.*, 1987; Katul and Chu, 1998; Nikora, 1999; Katul *et al.*, 2012), where $C'_{TKE} = 2C_s$. Furthermore, as argued elsewhere (Banerjee and Katul, 2013), $\sigma_u^2 \approx \sigma_v^2 + \sigma_w^2$ and thus $E_{tke}(k) \approx E_u(k)$ for $k < k_a$ in the ASL.

To summarize,

$$E_u(k) = \begin{cases} C'_{TKE}\,{u_*}^2\,k^{-1}, & \text{if } kz \le 1, \\ C_o\,\bar{\epsilon}^{2/3}\,k^{-5/3}, & \text{otherwise.} \end{cases} \tag{23}$$

A further discussion about the k^{-1} power law is necessary at this point. Specifically, a k^{-1} scaling at low wave numbers (k) for the streamwise turbulent velocity spectrum ($E_u(k)$) has been prevalent in turbulence literature since the early 1950s and across many experiments and simulations (Tchen, 1953, 1954; Klebanoff, 1954; Hinze, 1959; Pond *et al.*, 1966; Bremhorst and Bullock, 1970; Panchev, 1971; Bremhorst and Walker, 1973; Perry and Abell, 1975, 1977; Korotkov, 1976; Bullock *et al.*, 1978; Hunt and Joubert, 1979; Kader and Yaglom, 1984; Perry *et al.*, 1986, 1987; Turan *et al.*, 1987; Erm *et al.*, 1987; Perry and Li, 1990; Erm and Joubert, 1991; Kader and Yaglom, 1991; Yaglom, 1994; Katul *et al.*, 1996; Katul and Chu, 1998; Jimenez, 1999; Nikora, 1999; Katul *et al.*, 2012; Calaf *et al.*, 2013; Yang *et al.*, 2014), for both wall-bounded flows and ASL turbulence. However, a few studies have not observed a clear k^{-1} scaling or have argued against its existence in the unstably stratified ASL (Kaimal, 1978; Antonia and Raupach, 1993; Morrison *et al.*, 2002) and others have found its existence only under certain constraints (Nickels *et al.*, 2005), including very high Reynolds number and $z/\delta < 0.02$. Here, the k^{-1} spectrum is assumed to extend from $k \ge 1/H$ to $kz \le 1$,

where $H = \alpha\delta$ and $\alpha\delta$ is a measure of the largest size of eddies. Below $k = 1/H$ (i.e. at very large scales), the spectrum can be assumed to be flat, i.e. a constant value $(C'_{\mathrm{TKE}}\, {u_*}^2\, (1/H)^{-1})$ determined from the continuity requirement at $k = 1/H$. This assumption leads to a value of $\alpha = 1$, thereby retaining some energy in the very-large-scale motion, and eliminates the need to have a parameter (α) susceptible to fitting exercises. Hence, unless otherwise stated, $\alpha = 1$. Experimental datasets for near-neutral conditions appear to support this assumption, such as the $E_u(k)$ reported in Perry *et al.* (1986). It is important to note that this formulation for Zone I assumes C_s to be constant and the three regimes $-5/3$, -1 and flat spectrum hold. It is also to be noted that, although the spectral solution here might not be the most accurate representation, given that the spectrum might have some curvature at the intersection of the different domains and $E_u(k)$ has been assumed to be approximately equal to $E_{\mathrm{tke}}(k)$, it allows analytical tractability and provides a physical basis to expand Townsend's hypothesis to mildly unstably stratified flow as shown later.

2.5. Formulation for Zone II

While evaluating Eq. (20), it was assumed that C_s is approximately constant, thereby explaining the -1 power law in $E_u(k)$. However, beyond moderately unstable (e.g. $-\zeta > 0.5$), the assumptions that $E_{\mathrm{tke}}(k) \approx E_u(k)$ and the existence of a -1 power law for $kz < 1$ might be questionable, given the dependence of C_s on ζ.

As a first step to address these issues, the form of $E_{\mathrm{tke}}(k)$ at $kz < 1$ is still assumed to be a power law, as used to derive Eq. (22). Moreover, the simplified power expression for $C_s = p\,(\zeta)^q$ is now used, instead of a constant C_s. The modified form of Eq. (22) now becomes

$$\frac{a_1 z^{-3-b_1}}{3+b_1} = \frac{u_*^2}{z^2}\frac{p\, z^q}{L^q}, \tag{24}$$

which upon simplification yields $b_1 = -1 - q = -1.6 \approx -5/3$ and $a_1 = (2-q)u_*^2\, p/L^q$. This result is rather interesting, because it supports the hypothesis that another extended $-5/3$ scaling law, instead of the -1 scaling law, might be applicable at $kz < 1$, as indicated by the Kansas data (Kaimal and Finnigan, 1994), though this $-5/3$ scaling is not necessarily associated with an inertial subrange. In fact, two separate $-5/3$ regimes with a break in the vicinity of $kz = 1 - 4$ have already been reported for unstable conditions using previous long-term atmospheric surface-layer measurements (Kader and Yaglom, 1991). For analytical tractability, these two $-5/3$ regimes are not distinguished and are assumed to be approximated by a single power law with an exponent of $-5/3$. If the details of the transition from one $-5/3$ regime to another are known, then they can be incorporated.

Unfortunately, even with this simplification, the presence of a $-5/3$ alone at low k is not entirely prognostic, because (1) no clear estimate can be made about the low-wave-number break-point up till which the $-5/3$ scaling can be extended and assumed to be valid and (2) the precise shape of the spectrum is lacking in the vicinity of $-\zeta = 0.5$, where the -1 power law collapses and the $-5/3$ power law forms. Also, these two issues become compounded for large z, as the velocity statistics become quasi-isotropic, thereby violating the assumption that $E_{\mathrm{tke}}(k) \approx E_u(k)$ at low k in the spectral budget for $E_{\mathrm{tke}}(k)$.

However, this near-isotropic state may actually offer some guidance, because $E_w(k)$ can still be idealized via two regimes, a near flat-portion at low k and a $-5/3$ portion at larger k. It is argued here that the $E_u(k)$ spectrum may approach the $E_w(k)$ spectrum as the tendency towards isotropization is approached, which is likely to hold far from the boundary or at large z (and for $-\zeta > 0.5$). If it is assumed that the break-point of the now-constant to $-5/3$ regime spectrum is at $1/(\gamma_1 z)$, where γ_1 is assumed to be greater than unity (eddy sizes are larger than z at this break-point in $E_w(k)$), the E_u spectrum can be described as

$$E_u(k) = \begin{cases} C_{\mathrm{o}}\, \overline{\epsilon}^{2/3}\, (1/\gamma_1\, z)^{-5/3}, & \text{if } k\gamma_1\, z \le 1, \\ C_{\mathrm{o}}\, \overline{\epsilon}^{2/3}\, k^{-5/3}, & \text{otherwise,} \end{cases} \tag{25}$$

while the form of the flat spectrum $(k\gamma_1\, z \le 1)$ is obtained from the continuity requirement at $k = 1/\gamma_1\, z$.

To summarize, for instability conditions beyond moderate $(-\zeta > 0.5)$ and at distances sufficiently far from the boundary so that near-isotropic conditions are approached, the $E_u(k)$ shape is dramatically altered from near-neutral to moderately unstable conditions, resulting in a different formulation for σ_u/u_*. This domain of formulation and the associated spectral shape are marked on Figure 1 as Zone II. The dynamics in the intermediate zone (named zone III) are unknown and beyond the scope of the present work. In this zone, the $E_u(k)$ spectrum evolves from the spectral shape of the three-regime $-5/3$, -1, flat (in zone I) to the two-regime $-5/3$, flat spectra (in zone II).

2.6. The longitudinal velocity variance

For Zone I, integrating $E_u(k)$ from Eq. (23) from zero to infinity, the variance is

$$\sigma_u^2 = \int_0^{1/H} C'_{\mathrm{TKE}}\, {u_*}^2\, (1/H)^{-1}\, \mathrm{d}k + \int_{1/H}^{k_{\mathrm{a}}} C'_{\mathrm{TKE}}\, {u_*}^2\, k^{-1}\, \mathrm{d}k + \int_{k_{\mathrm{a}}}^{\infty} C_{\mathrm{o}}\, \overline{\epsilon}^{2/3}\, k^{-5/3}\, \mathrm{d}k. \tag{26}$$

Substituting $\bar{\epsilon} = (\phi_{\mathrm{m}}(\zeta) - \zeta)\, {u_*}^3/(\kappa\, z)$ and performing the integration,

$$\sigma_u^2 = C'_{\mathrm{TKE}}\, {u_*}^2 + C'_{\mathrm{TKE}}\, {u_*}^2\, \ln\left(\frac{H}{z}\right) + \frac{3}{2}\frac{C_{\mathrm{o}}\, {u_*}^2}{\kappa^{2/3}}\, (\phi_{\mathrm{m}}(\zeta) - \zeta)^{2/3}. \tag{27}$$

Normalizing σ_u^2 by ${u_*}^2$, Eq. (27) recovers Townsend's attached eddy hypothesis form (Marusic *et al.*, 2013):

$$\frac{\sigma_u^2}{{u_*}^2} = B_1(\zeta) - A_1(\zeta)\, \ln\left(\frac{z}{\delta}\right), \tag{28}$$

where

$$B_1 = \frac{3}{2}\frac{C_{\mathrm{o}}}{\kappa^{2/3}}\, (\phi_{\mathrm{m}}(\zeta) - \zeta)^{2/3} + C'_{\mathrm{TKE}}\, \ln(\alpha) + C'_{\mathrm{TKE}}, \tag{29}$$

and

$$A_1 \approx C'_{\mathrm{TKE}}, \tag{30}$$

are the intercept and slope, respectively. Recall that $C'_{\mathrm{TKE}} = 2C_s$ is dependent on ζ via Eq. (21), but only weakly in Zone I.

In summary, the derivation here unfolds some (but not all) necessary conditions for which MOST might explain distortions in σ_u^2/u_*^2 around its near-neutral state as specified by Townsend's hypothesis, due to thermal stratification. If the base-line neutral state of σ_u^2/u_*^2 involves a dimensionless variable z/δ (instead of being a constant as in σ_w/u_*), then under the restrictive conditions highlighted here, MOST may correct for deviations from this neutral baseline state via $A_1(\zeta)$ and $B_1(\zeta)$ due to finite ζ. This derivation is associated with a k^{-1} power-law scaling in $E_u(k)$ for $kz < 1$, which is not likely to hold for moderately unstable (i.e. $-\zeta > 0.5$) conditions and most definitely will not hold for approximate convective conditions (i.e. $-\zeta > 5$). Nonetheless, maintaining the $C'_{\mathrm{TKE}} = 2C_s$ dependence on ζ (instead of a constant) as in Eq. (21) allows the initial discussion of σ_u/u_*

scaling to be anchored to established norms to boundary layers in near-neutral conditions. Stated differently, the derivation here shows that if the shape of the spectrum of u is unaltered by ζ (specified in Zone 1) and if variations in ζ are primarily attributed to L instead of z, then a straightforward extension of Townsend's attached eddy hypothesis can explain variations in σ_u^2/u_*^2 via $A_1(\zeta)$ and $B_1(\zeta)$ due to finite ζ. The adequacy and robustness of this extension to Townsend's hypothesis will be discussed further. This derivation also makes it clear that, with increasing instability, if the shape of the u spectrum changes from its Zone I state and if the $-\zeta$ increases are due to either z or L, then a straightforward extension of Townsend's attached eddy hypothesis via $A_1(\zeta)$ and $B_1(\zeta)$ is likely to be insufficient, as is the case for Zone II.

For Zone II and with the large z assumption (but still in the ASL) and upon integrating the spectrum in Eq. (25), the longitudinal velocity variance is given by

$$\frac{\sigma_u^2}{u_*^2} = \left(1 + \frac{3}{2}\right) \frac{C_o}{\kappa^{2/3}} (\phi_m(\zeta) - \zeta)^{2/3} {\gamma_1}^{2/3}. \qquad (31)$$

Hence, if γ_1 is known, how σ_u/u_* varies with ζ for unstable to convective conditions can be predicted. There are a number of assumptions that complicate the determination of γ_1. The first pertains to the presence of two $-5/3$ power laws for small and large k instead of a single power law. The degree of separation in wave number space and the shape of the connecting spectrum between these two $-5/3$ exponents can certainly impact the numerical value of γ_1. Moreover, there are large uncertainties in the shape of the spectrum for scales much larger than $\gamma_1 z$ and a constant extension to $k = 0$ is oversimplistic at best.

3. Results

3.1. Comparison with laboratory experiments and the near-neutral limit (Zone I)

Before the effects of atmospheric (in)stability are discussed, the σ_u^2/u_*^2 scaling is first presented for the near-neutral case where $\phi_m(0) = \phi_T(0) = 1$. For Zone I, the shape of the spectrum predicted from the spectral budget can be found in Figure 1. Also, for these near-neutral stability conditions, the general log law (Marusic *et al.*, 2013) $\sigma_u^2/u_*^2 = B_1 - A_1 \ln(z/\delta)$ recovered from Eq. (28) is observed across several laboratory experiments, as discussed elsewhere (Banerjee and Katul, 2013). The estimates for $A_1 = 1.2$–1.4 and $B_1 = 1.6$–2.3 reported in Marusic *et al.* (2013) are reasonably recovered when $\alpha = 1$. Using a flat spectrum at $kH < 1$, the constant B_1 can be estimated as $B_{1a} = C_o/\kappa^{2/3}\,(1 + 3/2 + \ln(\alpha)) = 2.5$, which appears to be commensurate with the upper limit set by Marusic *et al.* (2013). The parameter A_1 is estimated as $A_1 \approx C_o/\kappa^{2/3}$, which with $C_o = 0.55$ and $\kappa = 0.4$ results in $A_1 \approx 1$. This estimate is again commensurate with the lower limit provided by Marusic *et al.* (2013).

To begin unfolding the effects of atmospheric stability on σ_u^2/u_*^2, consider the case in which C_s predicted from Eq. (21) is inserted into Eq. (22) without any modification (i.e. variations in ζ are assumed to originate from variations in L, not z) and the spectrum for the formulation for Zone I holds. The outcome of this exercise shows how the two parameters associated with Townsend's hypothesis for σ_u^2/u_*^2, namely the intercept B_1 and slope A_1, might be nonlinearly modified by ζ within the ASL (though, as earlier noted, Eq. (22) does not capture the spectral dynamics for Zones II and III correctly). Both parameters appear approximately constant up to $-\zeta < 0.5$ (i.e. Zone I) and then are predicted to increase dramatically as more unstable conditions are approached. In the neutral limit, they approach the values $B_1 = 2.5$ and $A_1 = 1$, respectively, as discussed earlier.

The derivation here also brings into focus why ζ is not a unique parameter explaining the variability in σ_u/u_* as predicted by MOST for σ_w/u_*. As mentioned earlier, it has been known for some time now that δ/L is a more dominant parameter affecting σ_u/u_* for ASL flows (Lumley and Panofsky, 1964; Panofsky *et al.*, 1977). The spectral budget here predicts how the dimensionless groups $\zeta = z/L$ and $z/(\alpha\delta)$ describe σ_u/u_*, at least for the conditions when $\zeta = z/L$ variations are dominated by L instead of z and the onset of the -1 power law in $E_u(k)$ for $kz < 1$ is not nullified by thermal stratification.

For illustration purposes only, Figure 2 shows computed σ_u/u_* varying with both z/δ and $\zeta = z/L$ for $\alpha = 1.0$ using a straightforward extension of Townsend's hypothesis with B_1 and A_1 modified by ζ. The individual scaling behaviour of σ_u/u_* with ζ and δ/L is also shown in the figure and the model is again found to produce a 1/3 scaling behaviour in the limits of large $|\delta/L|$ and $|z/L|$. It is to be noted that that z is fixed at 5 m, $-\zeta$ is varied from 10^{-3} to 10 and δ is varied from 10^2 to 10^3 m. In terms of asymptotic behaviour in the neutral limit, the model converges to $\sigma_u/u_* = 2.3$ and the functional form by Panofsky *et al.* (1977) converges to $\sigma_u/u_* = 2.0$, which corroborates to the range 2–3 reported in the literature (Lumley and Panofsky, 1964; Hsieh and Katul, 1997; Kader and Yaglom, 1990). Note the increase in σ_u/u_* with increasing δ for fixed z, which is also observed in figure 3 of Banerjee and Katul (2013). Furthermore, for fixed δ, the increase in σ_u/u_* is also observed in the surface plot with increasing $|\zeta|$.

Functional forms of the variation of σ_u/u_* empirically fitted to several experiments have been provided by Panofsky *et al.* (1977) as $\sigma_u/u_* = [4 + 0.6(\delta/(-L))^{2/3}]^{1/2}$. Using another expansive data set, Wilson (2008) provided a modification to Panofsky's form by incorporating the z and δ variation as $\sigma_u/u_* = ([4 + 0.73(\delta/(-L))^{2/3}][1 - (z/\delta)^{0.25}])^{1/2}$. These empirical functions represent a large corpus of data on variations in σ_u/u_* and serve as a logical basis for evaluating the proposed formulation.

Because of the constraint $z \ll \delta$, which is not too different from the limit in Nickels *et al.* (2005) to ensure the onset of a -1 power law in the longitudinal velocity spectrum, the comparisons are shown for a reasonably small $z = 5$ m (i.e. $z/\delta < 0.02$) in Figure 3(a); these comparisons appear surprisingly reasonable even for moderately unstable conditions $-\zeta > 1$, given the lack of any tunable parameter here. However, for a high (separated by an order of magnitude) value of $z = 50$ m (i.e. $z/\delta > 0.02$), the comparisons between the models remain strongly correlated but biased by a multiplier, as shown in Figure 3(b). Recall that, when deducing Eq. (22), variations in ζ were momentarily assumed to originate from variations in L, not z. This simplification allowed polynomial matching to recover the -1 power law in the spectra at the expense of ignoring large variations in z when determining $C_s(\zeta)$. This deficiency is discussed later, after comparisons with a recent field experiment, the Advection Horizontal Array Turbulence Study (AHATS), is presented.

3.2. Comparisons with the AHATS field experiment

Assumptions made in deriving the spectral budget are now explored using ASL data collected as part of AHATS, conducted near Kettleman City, CA, USA from 25 June 2008–17 July 2008 (Salesky *et al.*, 2013). Here, data from the AHATS profile tower is considered, where velocity and temperature measurements were collected using Campbell Scientific CSAT-3 triaxial sonic anemometers at heights of $z = 1.51$, 3.30, 4.24, 5.53, 7.08 and 8.05 m. Raw data were sampled at 60 Hz, then down-sampled to 20 Hz during preprocessing. The data were divided into blocks of 27.3 min or $32\,768 = 2^{15}$ data points per block to permit the use of fast Fourier transforms in spectral density estimation. The coordinate system was aligned with the mean wind direction, so that $U_2 = 0$ for each block, as noted earlier. Only blocks of data with wind angles of $|\alpha_w| \leq 45^\circ$ were included in the analysis. Several quality-control criteria were employed during the pre-processing. Blocks of data that exhibited more than a 30% deviation of $\phi_w = \sigma_w/u_*$ from the value predicted by

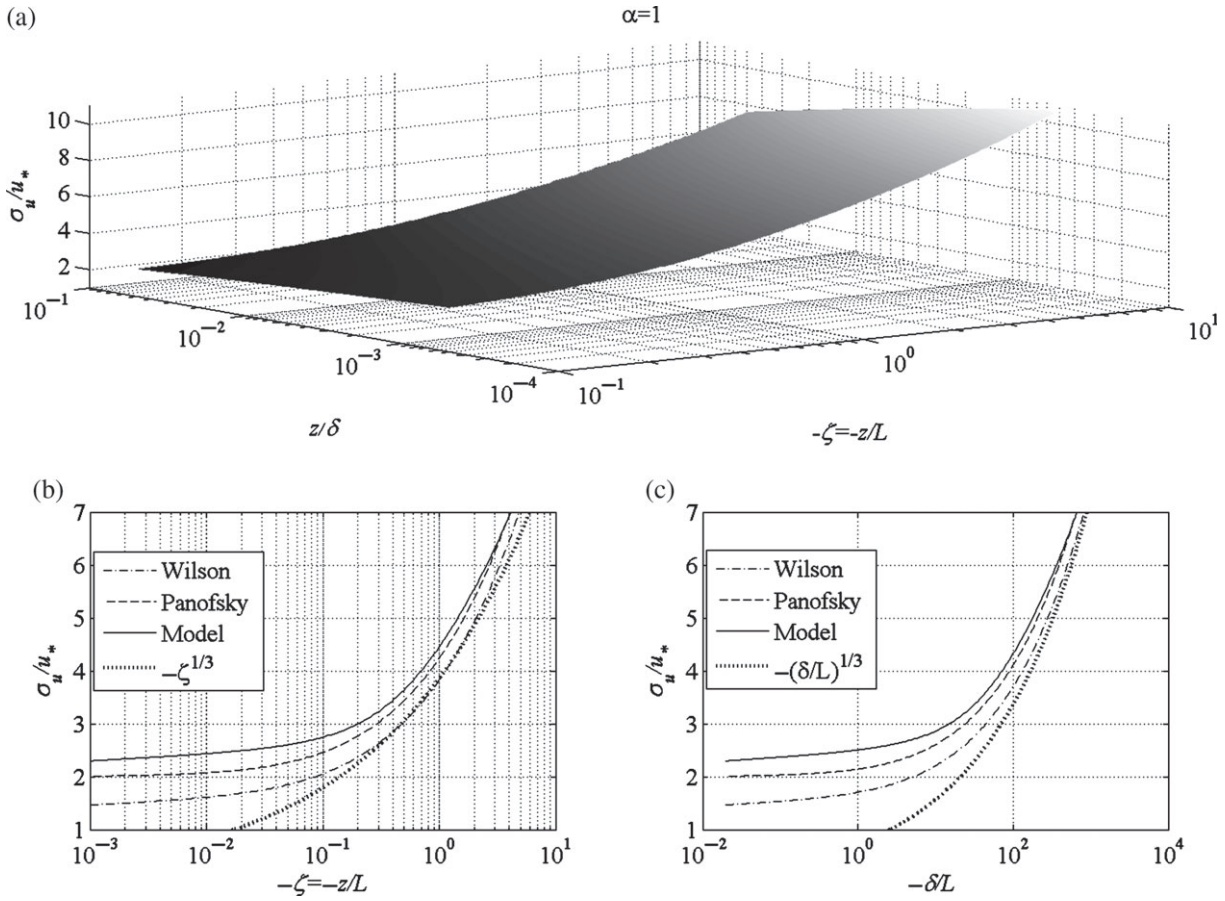

Figure 2. (a) The computed variation of σ_u/u_* with z/δ and $-\zeta = z/L$ at $\alpha = 1$ and $z = 5$ m, shown as a surface plot. This formulation is based on the extrapolation of the formulation for Zone I (i.e. a straightforward extrapolation of Townsend's hypothesis with B_1 and A_1 modified by ζ). (b) Variation of σ_u/u_* with $-\zeta = -z/L$. Similar scaling behaviour obtained from the functional forms described in Panofsky *et al.* (1977) and Wilson (2008) is also shown. (c) Variation of σ_u/u_* with $-\delta/L$. Similar scaling behaviour obtained from the functional forms described in Panofsky *et al.* (1977) and Wilson (2008) is also shown. The $(-\zeta)^{1/3}$ and $(-\delta/L)^{1/3}$ scaling in the semi-log representation are depicted in both (b) and (c) for reference.

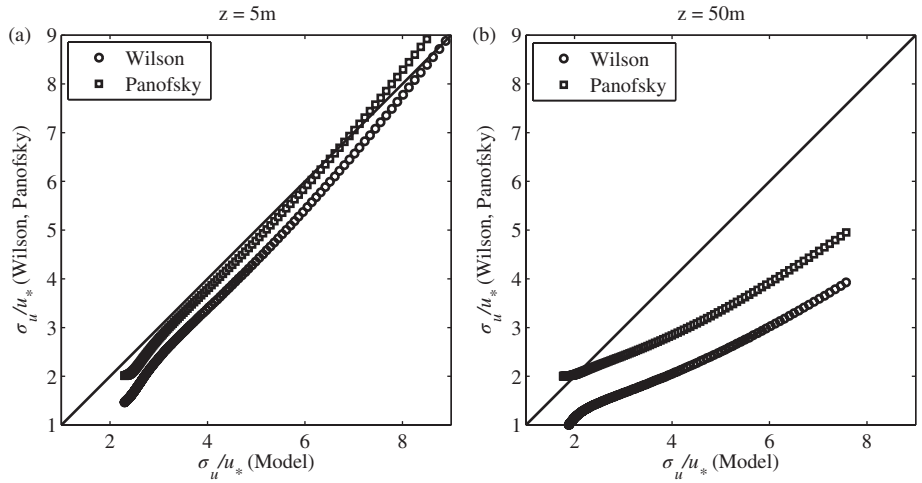

Figure 3. Comparisons between model estimates and the functional forms provided by Wilson (2008) and Panofsky *et al.* (1977) for two different heights: (a) $z = 5$ m and (b) $z = 50$ m.

MOST were discarded (Lee *et al.*, 2004). To minimize the effects of non-stationarity on the calculated statistics, non-stationary ratios (Vickers and Mahrt, 1997) for the streamwise (RNu), cross-wind (RNv), and vector (RNS) velocity components were examined for each period. Blocks of data were excluded from the analysis if RNu, RNv or RNS ≥ 0.5. Blocks of data were also excluded if the measured $u_* \leq 0.1\,\mathrm{m\,s^{-1}}$ or measured $\rho c_p \overline{w'T'} \leq 10\,\mathrm{W\,m^{-2}}$ (Högström, 1988). Finally, because MOST requires the assumption that the turbulent fluxes do not vary with z within the ASL, periods where either momentum or heat flux varied more than 20% with z, as quantified by the coefficient of variation across z, were discarded.

The mean velocity and temperature gradients were calculated by fitting a second-order polynomial in $\ln z$ to the calculated mean profiles, e.g. $U(z) = Af_m \ln z + Bf_m (\ln z)^2 + Uf_0$, where Af_m, Bf_m and Uf_0 are constants determined through linear regression fitting. The polynomial fit can then be differentiated to determine the mean gradient by

$$\frac{\partial U}{\partial z} = \frac{Af_m}{z} + \frac{2Bf_m \ln z}{z}. \tag{32}$$

The mean turbulent kinetic energy dissipation and temperature variance dissipation rates were simultaneously estimated by linear regression of the compensated second-order structure functions,

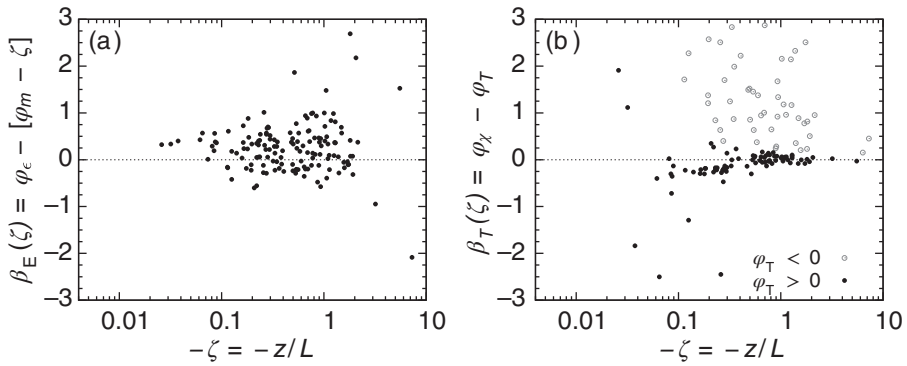

Figure 4. Local imbalance of (a) the turbulence kinetic energy budget and (b) the temperature variance budget, plotted as a function of the MOST stability variable $-\zeta$. Note that in (b), runs with counter-gradient heat fluxes ($\phi_T < 0$) are plotted separately.

e.g.

$$r_1^{-2/3} D_{11}(r_1) = c_2 \epsilon^{2/3} = a r_1 + b \tag{33}$$

for spatial lags r_1 in the range $0.2 \leq r_1 \leq 2.0$ m (Salesky *et al.*, 2013).

Here, r_1 is determined from Taylor's frozen turbulence hypothesis (Taylor, 1938). In an analysis of deviations from MOST, Salesky and Chamecki (2012) found that best-fitting curves to $\phi_m(\zeta)$ and $\phi_T(\zeta)$ from the AHATS data set were similar to the Businger–Dyer empirical form. The local balance assumptions for the TKE and temperature variance budgets are also examined here using the AHATS data. In Figure 4, the local imbalance (i.e. dissipation − production) of the TKE (β_E) and temperature variance (β_T) budgets are presented in panels (a) and (b), respectively. For unstable conditions, the imbalance of the TKE budget in Figure 4(a) scatters around $\beta_E = 0$. In Figure 4(b), the imbalance in the temperature variance budget β_T also scatters around zero for the majority of the data runs. However, data points with large values of β_T occurred for runs with $\phi_T < 0$, i.e. a countergradient heat flux. Discussions of the local imbalance of the TKE budget can also be found for other recent studies (Wilson, 2008; Salesky *et al.*, 2013).

Notwithstanding these issues, it can be surmised here that, for unstable and near-neutral conditions, the TKE budget is close to a local balance on average, i.e. on average $\beta E(\zeta) \approx 0$ (Salesky *et al.*, 2013). Spectra from AHATS, shown in Figure 5, were calculated using the 60 Hz data (the inertial range is not really present in the 20 Hz data) using periods of approximately 54.8 min. The use of such long periods allowed an extension of the measured spectra to a small wave number range, which is needed to assess the slope in the $kz < 1$ range. Each spectrum was first normalized by $C_0\overline{\epsilon}^{2/3}$ so as to collapse the inertial range and then spectra were averaged in bins of ζ, as indicated in the figure. Figure 6(a) and (b) do suggest a transition from k^{-1} to $k^{-5/3}$ scaling for $kz < 1$ with increasing instability for $E_{\rm TKE}$ and E_u, respectively, consistent with the predictions here for Zones I and II. To investigate the spectral scaling further, compensated spectra using $k^{5/3}$ are also shown in Figure 6(c) and (d) and spectra using k^1 are shown in Figure 6(e) and (f).

The measured spectra in most runs from AHATS support the existence of a decade of −1 power-law scaling in $E_u(k)$ and $E_v(k)$ but not $E_w(k)$ at $kz < 1$ for small $-\zeta < 0.5$ (consistent with theoretical predictions for Zone I). Also, the AHATS measured spectra suggest the collapse of a −1 power law in $E_u(k)$ and $E_v(k)$ and the initiation of an extended −5/3 power law beyond $kz < 1$ around an atmospheric stability limit $-\zeta > 0.5$, as predicted from $C_s(\zeta)$ in Zone II) and shown in Figure 6. The finding that the $E_v(k)$ spectrum is similar to the $E_u(k)$ spectrum ($E_u(k) = E_v(k)$) supports further the assumption that $E_u(k) + E_v(k) \gg E_w(k)$ and hence $E_{\rm tke} = (1/2)(E_u(k) + E_v(k) + E_w(k)) \approx E_u(k)$ at low k. In fact, the assumption of $\sigma_u^2 \approx \sigma_v^2 + \sigma_w^2$ and thus $E_{\rm tke}(k) \approx E_u(k)$ for $k < k_{\rm a}$ in the ASL can be also tested using the AHATS data. Figure 6 shows a one-to-one comparison between σ_u^2 and $\sigma_v^2 + \sigma_w^2$ computed from AHATS data and the assumption can be deemed to be fair.

As atmospheric instability increases beyond $-\zeta > 0.5$, two $k^{-5/3}$ regions can be identified in $E_{\rm TKE}$ in Figure 6(c) (i.e. in pre-multiplied form), consistent with measurements reported elsewhere (Kader and Yaglom, 1991) for unstable ASL conditions. As noted earlier, these two separated −5/3 regimes are 'lumped' together into a single regime here for analytical tractability in Zone II and the uncertainties associated with such simplifications are absorbed in γ_1.

To illustrate the role of δ on σ_u/u_* from the AHATS, σ_u/u_* was calculated for morning periods from 0800–1000 PDT (1500–1700 UTC) (assumed to have smaller δ) and afternoon periods from 1400–1600 PDT (2100–2300 UTC) (assumed to have larger δ) using the straightforward extension of Townsend's hypothesis with stability-dependent A_1 and B_1. Because a direct measurement of δ was not available, the average boundary-layer depth for morning and afternoon periods was estimated using a slab model described in Juang *et al.* (2007) and discussed in the Appendix. From the slab model, values of $\delta = 289 \pm 31$ m for the morning (0800–1000 PDT) period and $\delta = 836 \pm 37$ m for the afternoon (1400–1600 PDT) were obtained. The afternoon estimate of δ from the slab model was found to be consistent with the value of $\delta = 780 \pm 130$ m estimated visually from plots of the afternoon sounding (typically taken around 1400 PDT (2100 UTC)) available from the National Center for Atmospheric Research (NCAR) project website.

For each of these distinct δ and at a given z, the σ_u/u_* approximately collapse on to a single curve as ζ varies. Consistent with earlier model calculations shown in Figure 2(a), the afternoon σ_u/u_* is found to be higher than its morning counterpart for the same ζ, signifying the effects of δ at a fixed z. Noting that α was pre-set to unity in all calculations, the variations at both z and δ are reasonably predicted by the model, as shown in Figure 7. This agreement is also not a consequence of any artificial self-correlation arising from u_* impacting the dependent and independent variables jointly, as measured and modelled dimensional σ_u also agree (not shown). However, the model is found to be biased by about 15% with a coefficient of determination exceeding 0.7. It is evident that the modelled σ_u/u_* overpredict the measurements for the smaller δ (or morning) values, at least when compared with the larger δ case. This bias may already be hinting that the modelled $E_u(k)$, with its predicted −1 power-law form (as derived for Zone I), is not correctly reproducing the measured $E_u(k)$ in Zone II as expected when a straightforward extension of Townsend's hypothesis with stability-dependent A_1 and B_1 is employed in this zone. Recall that the AHATS spectra also show a shift from a −1 to a −5/3 exponent in $E_u(k)$ with increasing instability.

3.3. *Comparisons with literature data*

Two different types of field data, compiled in Panofsky *et al.* (1977), are now discussed against model predictions in Figure 8,

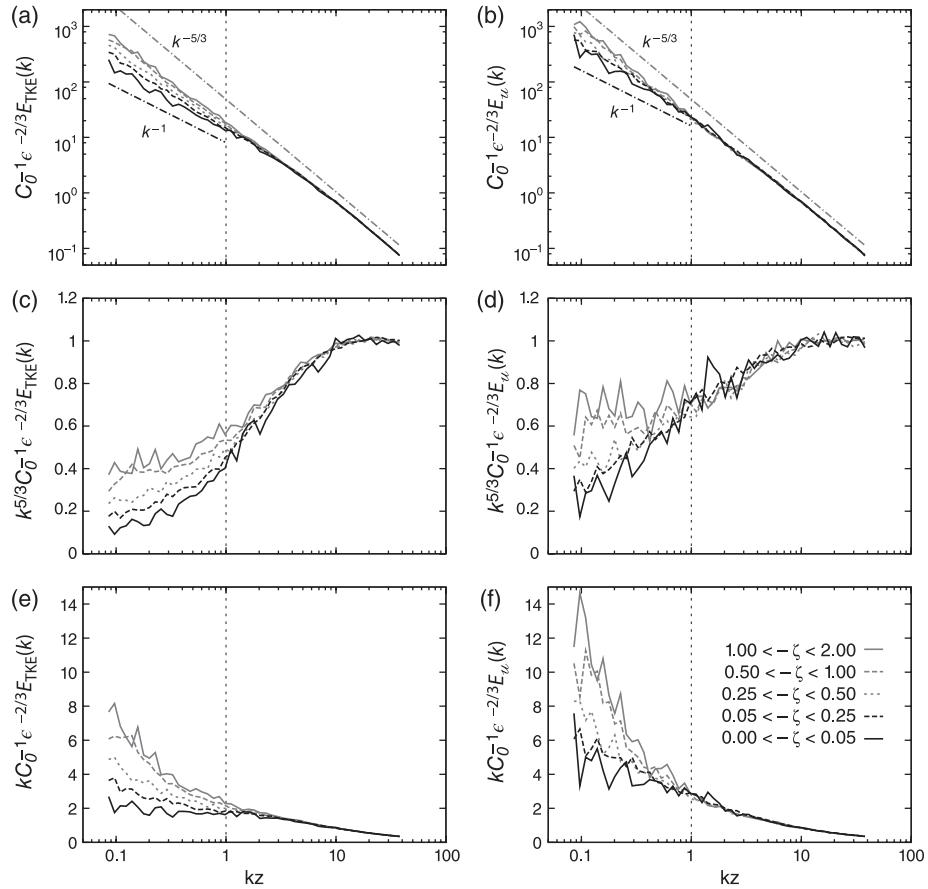

Figure 5. (a)–(b) $E_u(k)$ and $E_{\text{tke}}(k)$ spectra from AHATS experiment averaged over bins of $-\zeta$ illustrating the existence of a -1 power-law in the large scales for near neutral conditions transitioning to a $-5/3$ power-law for strongly unstable conditions. Panels (c)–(f) show compensated versions of the spectra to emphasize the existence of the -1 and $-5/3$ scalings for $kz < 1$.

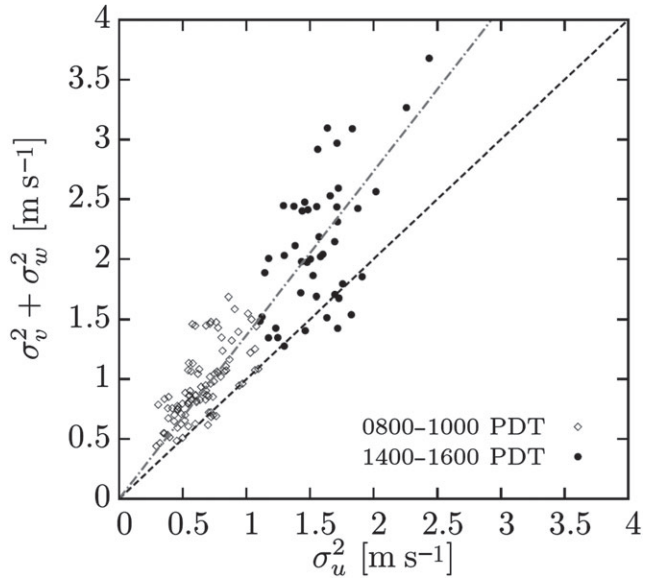

Figure 6. The fit shows that Assesment of assumption $\sigma_{v^2} + \sigma_{w^2} \approx \sigma_{u^2}$ using AHATS data. Black dashed line represents assumption $\sigma_{v^2} + \sigma_{w^2} \approx \sigma_{u^2}$ while gray dot-dashed line represents best fit given by $\sigma_{v^2} + \sigma_{w^2} \approx 1.37\,\sigma_{u^2}$.

when using Eq. (30) with C_s given by Eq. (21). For clarity, Figure 8 shows the comparisons between model and measurements for the tower and aircraft data reported in Panofsky *et al.* (1977). The tower data, measured at different heights (ranging from 4–32 m, but precise heights not reported) are represented here by an average $z = 18$ m and the model calculations assume $\alpha = 1$ (i.e. no tunable parameter). The tower data are reasonably predicted by the model for all stability (unstable) conditions. The aircraft data, however, are found to be overpredicted (again consistent with the bias noted for the AHATS experiment for smaller δ). To be clear, a number of cautionary notes about the aircraft data must be highlighted in this comparison. The aircraft data were analyzed in Panofsky *et al.* (1977) by assuming $\sigma_u = \sigma_v$; the measurement heights were sufficiently large (>100 m) that neglecting Coriolis effects or the flux transport terms in the TKE or, equally importantly, the temperature variance budgets, as done here, may be questionable. Furthermore, the assumption that $E_{\text{tke}}(k)$ is dominated by $E_u(k)$ clearly breaks down at these heights, where the degree of anisotropy is far weaker when compared with the tower measurements collected near the surface. Notwithstanding these issues, it is to be noted that, when $\alpha = 1$ is replaced with $\alpha = 0.25$, the proposed model can reproduce the reported aircraft σ_u/u_* to high fidelity. However, such a small α (or any other empirical reduction to it with increasing z) indicates significant reductions in low-frequency energy that cannot be explained theoretically by the current solution to the spectral budget. That is, significant differences exist between the σ_u/u_* formulations for Zones I and II (or Eqs (28) and (31)), reflecting fundamental differences in the scaling laws describing the shapes of the energy spectra for these two zones. This will be discussed further in subsequent sections.

Interestingly, a one-third scaling of σ_u/u_* with ζ for a fixed boundary-layer height has been prevalent in some studies reporting $\sigma_u/u_* = 2.7(1 - 3\zeta)^{1/3}$ (Panofsky and Dutton, 1984; Hsieh and Katul, 1997). The spectral budget model is found to retrieve that 1/3 scaling for large $-\zeta$ reasonably, as shown in Figure 9, though such a 1/3 scaling is known to be contaminated by self-correlation, given that u_* variations impact dependent and independent variables here. A comparison between measured and modelled σ_u was repeated (not shown) and the agreement between them was commensurate with the AHATS agreements.

The proposed scaling law and the model are also found to represent the data over grass and bare soil reasonably, although the grassland data are found to be more scattered, due to the fact that they were collected in non-ideal ASL conditions (within a

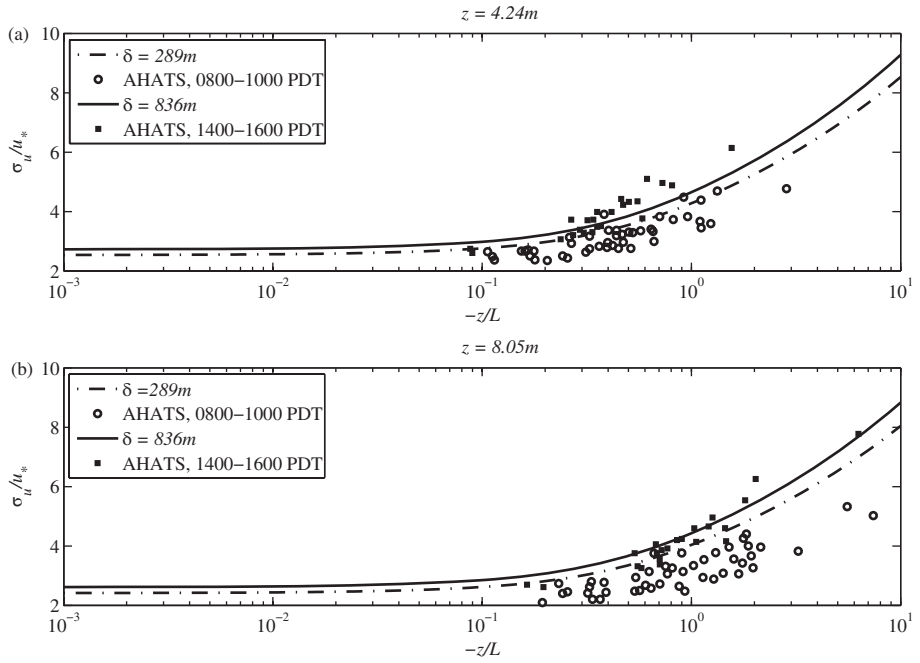

Figure 7. Measured σ_u/u_* from the AHATS experiment for two different heights of the boundary layer ((a) and (b)) in the morning and the afternoon, for two different heights of measurement (z). The data show variation with $-\zeta$ as well as δ. Both variations appear to be predicted by the model depicted by solid and dash–dotted lines for two different δ values for morning ($\delta = 289$ m) and afternoon ($\delta = 836$ m).

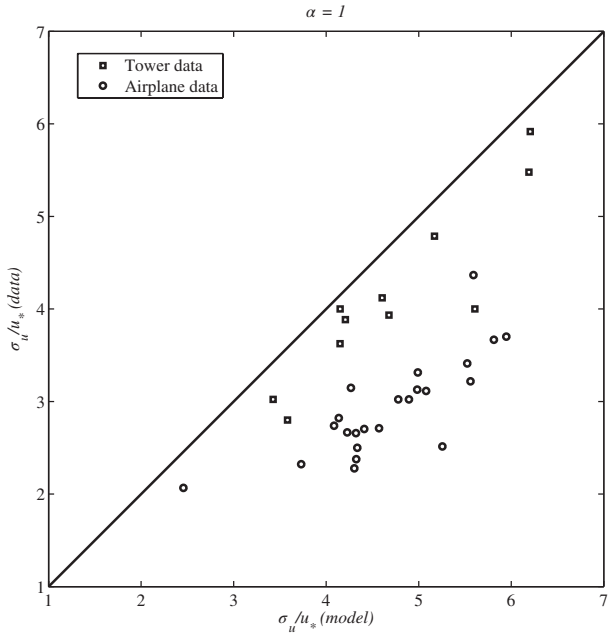

Figure 8. Comparisons between modelled and measured σ_u/u_* using data from Panofsky *et al.* (1977) for the tower and aircraft platforms. This model is represented by a single $\alpha = 1$.

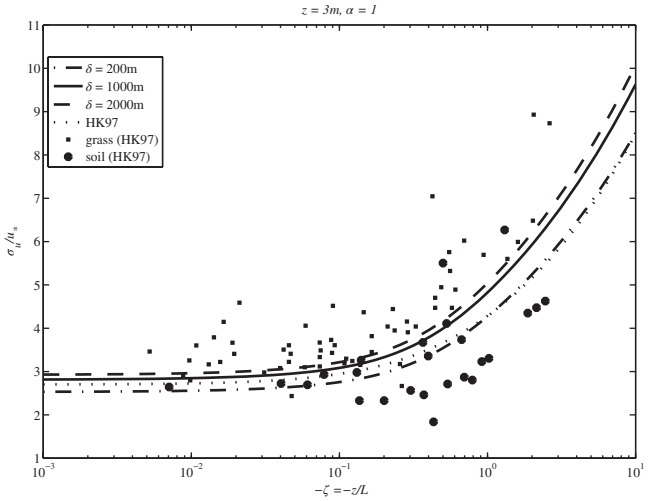

Figure 9. Variation of σ_u/u_* with $-\zeta = -z/L$ for $\alpha = 1.0$ and three different $z/\delta = 0.05$, 0.01 and 0.005. The data over grass and soil from Hsieh and Katul (1997) (HK97) are superimposed on the figure, also showing the 1/3 power-law scaling relation proposed in Hsieh and Katul (1997) as $\sigma_u/u_* = 2.7(1 - 3\zeta)^{1/3}$.

large forest clearing). To summarize, no unique dimensionless group describes variations in σ_u/u_* for the unstable ASL, but there are a few length-scales (at minimum z, $\alpha\delta$ and L) that must be accommodated. Even in the near-neutral ASL, σ_u/u_* varies with z/δ as earlier shown by Townsend, perhaps explaining why the scatter in field data is large for such near-neutral conditions. Also, in contrast to the scaling proposed by Panofsky *et al.* (1977), ζ remains an essential variable, needed here to explain some of the variations in σ_u/u_*, at least for very small z/δ, lending further support to the proposed amendment by Wilson (2008).

3.4. *Results pertaining to Zone II*

It was assumed before that variation in ζ originated primarily from L while evaluating Eq. (20). This assumption unexpectedly reproduced σ_u/u_* well even when $-\zeta > 0.5$, provided z was small (as expected from tower measurements). However, when comparing with aircraft measurements, this assumption results in the model being biased for large z, as shown in Figures 8 and 3(b). The fate of the model for somewhat larger z and $-\zeta$ but still for $z/\delta < 0.1$ (i.e. flow within the ASL) requires further examination, as has already been discussed in section 2.5. The final form of σ_u/u_* from this discussion (Zone II) can be found in Eq. (31). This formulation is valid for $-\zeta > 0.5$ (Zone II), where z is sufficiently large. The need for a large z separate from the requirement of $-\zeta > 0.5$ is to ensure near-isotropic conditions become prevalent (i.e. $E_w(k)$ and $E_u(k)$, as well as their wave number integrations, are commensurate) away from the boundary, but otherwise maintaining all the assumptions in the idealized ASL. This formulation is tested against the functional forms proposed by Panofsky *et al.* (1977) and Wilson (2008) and the aircraft data provided in Panofsky *et al.* (1977) and shown in Figure 10. It is found that a value of $\gamma_1 = 2$ is a reasonable estimate, i.e. the inertial behaviour is found to

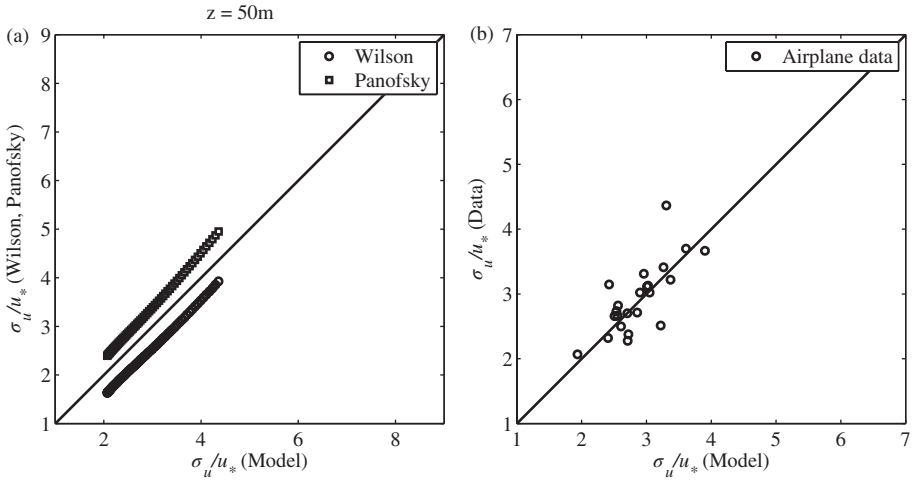

Figure 10. (a) Comparisons between predictions from Eq. (31) and the functional forms provided by Panofsky *et al.* (1977) and Wilson (2008) using $\gamma_1 = 2$. (b) One-to-one comparison with aircraft data provided by Panofsky *et al.* (1977).

continue up to a height commensurate with twice the observation height when z is large and $\zeta > 0.5$ (Zone II). Interestingly, this estimate appears to be consistent with variations in the spectral peaks of $kE_w(k)$ reported for the Kansas experiments. For example, Kaimal and Finnigan (1994) report that the spectral peaks inferred from measured $kE_w(k)$ when normalized by their near-neutral limit (=$fp_w(\zeta)$) are given as $fp_w(\zeta) = (1 - 0.7|\zeta|)^{-1}$ when $-\zeta < 1$ and $= fp_w(\zeta) = 3.23$ when $1 < -\zeta < 0.1\delta/L$. That is, as isotropic conditions are approached away from the boundary (i.e. $E_w(k) \approx E_u(k)$), which is expected in the large z limit, the Kansas data do suggest that $1 < \gamma_1 < 3.23$ (as inferred from $E_w(k)$), consistent with the intermediate $\gamma_1 = 2$ found here. Recall that the $E_u(k)$ spectrum assumed here (i.e. flat for $k < (\gamma_1 z)^{-1}$ and exhibiting a $-5/3$ scaling for $k > (\gamma_1 z)^{-1}$) has its well-defined spectral peak at $k = (\gamma_1 z)^{-1}$ where $kE_u(k)$ is maximum, consistent with its $kE_w(k)$ counterpart when z is large and $-\zeta > 0.5$. Also, it is to be noted that γ_1 is impacted by the assumption of a single $-5/3$ exponent as given by Eq. (24), an assumption not supported by the AHATS spectra in Figure 6.

4. Conclusion

A spectral budget method has been discussed to explain the characteristics of the normalized streamwise turbulent intensity (σ_u^2/u_*^2) under an unstably stratified atmosphere. This budget showed why a straightforward extension of Monin–Obukhov similarity theory (MOST) to σ_u^2/u_*^2 is inadequate. Analytical solutions to this spectral budget were possible for two limiting conditions: (1) $z/\delta < 0.02$ and $|z/L = \zeta| < 0.5$ (labelled as Zone I) and (2) $0.02 \ll z/\delta < 0.1$ and $|\zeta| > 0.5$ (labelled as Zone II). The $z/\delta = 0.02$ limit was derived independently from laboratory studies (near-neutral conditions) and was found to be reasonable here and the $-\zeta = 0.5$ limit was inferred from Figure 1, while spectral analysis of the AHATS data also indicated a similar trend. The first condition ensured the onset and maintenance of a -1 power law in $E_u(k)$ at low k for mildly unstable conditions. The second condition is associated with a deterioration of the -1 power law in $E_u(k)$ and its eventual replacement with a $-5/3$ scaling beyond $kz < 1$. The σ_u comparisons have been checked for self-correlation and it has been found that any self or spurious correlation is not the cause of the fair agreements.

The work here showed that σ_u^2/u_*^2 is found to conform to the logarithmic scaling anchored to Townsend's attached eddy hypothesis for near-neutral conditions (or Zone I), while the coefficients of this log law are found to be modified by MOST for mildly unstable conditions. The required low $z/\delta \ll 1$ condition for observing a -1 power law is compatible with laboratory measurements by Nickels *et al.* (2005) for neutral boundary-layer flows. That is, Townsend's attached eddy hypothesis, the height conditions promoting the -1 power law ($z/\delta < 0.02$) and the MOST expansion for non-neutral flows to mildly unstable in the ASL are all interconnected. Interestingly, the σ_u^2/u_*^2 derived for $z/\delta < 0.02$ and $|\zeta| < 0.5$ (Zone I) appears to be robust to variations in $|\zeta| < 0.5$ and agreement with measurements and other empirical models was surprisingly found to hold up to $-\zeta = 10$ for tower measurements, where z was small. In the case of higher z, but still $z/\delta < 0.1$ and a finite $-\zeta > 0.5$ (Zone II), the longitudinal spectrum loses its -1 scaling, consistent with the laboratory findings in Nickels *et al.* (2005), and follows an approximate $-5/3$ scaling at low wave numbers, consistent with Kader and Yaglom (1991), though this exponent is not connected to the inertial subrange. Using this asymptotic argument for $z/\delta < 0.1$ and a finite $-\zeta > 0.5$, a different model for σ_u/u_* was derived and shown to agree with earlier models and aircraft data for those conditions. Naturally, 'stitching' these two limiting conditions via some *ad hoc* function is possible (e.g. Zone III), though such stitching does not guarantee correct predictions of $E_u(k)$ at $kz < 1$. Progress on how to transition from one formulation to another for σ_u/u_* can greatly benefit from large eddy simulation runs, where z, L and δ are allowed to vary. Perhaps more broadly, the fact that $E_u(k)$ does not exhibit a single 'canonical' shape across all z, L and δ may explain the lack of 'non-universal' form in σ_u/u_* when all these length-scales are varied simultaneously.

Acknowledgements

T. Banerjee and G. Katul acknowledge support from the National Science Foundation (NSF-EAR-1013339, NSF-AGS-1102227), the United States Department of Agriculture (2011-67003-30222), the US Department of Energy (DOE) through the office of Biological and Environmental Research (BER) Terrestrial Ecosystem Science (TES) Program (DE-SC0006967) and the Binational Agricultural Research and Development (BARD) Fund (IS-4374-11C). The AHATS data were collected by NCAR's Integrated Surface Flux Facility.

Appendix

Discussion on the details of the slab model used to estimate boundary-layer depth in AHATS

The average boundary-layer depth for morning and afternoon periods was estimated using a slab model described in Juang *et al.* (2007). Briefly,

$$\frac{\mathrm{d}\delta}{\mathrm{d}t} = \frac{(\overline{w' T'_{Ps}} - \overline{w' T'_{P\delta}})}{\gamma\, \delta}, \tag{A1}$$

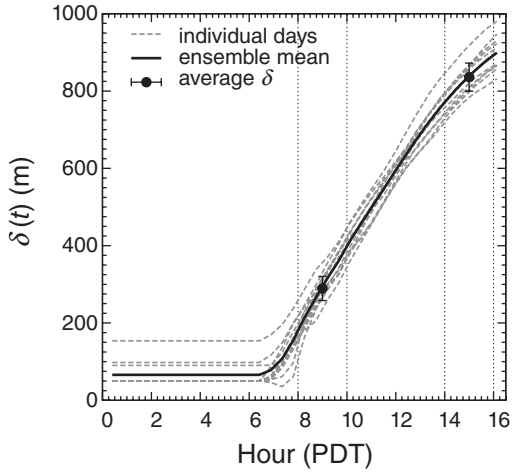

Figure A1. Predicted time evolution of boundary-layer height δ from the slab model for each day, together with the ensemble mean.

where $\overline{w' T'_{Ps}}$ and $\overline{w' T'_{P\delta}}$ represent the turbulent sensible heat fluxes at the surface and at the top of δ and γ is the local lapse rate of the mean slab potential temperature $\overline{T}_P$ just above δ. Invoking the standard assumption that $\overline{w' T'_{P\delta}} = -\beta \overline{w' T'_{Ps}}$ (Tennekes, 1973), setting $\beta = 0.3$ (Kim and Entekhabi, 1998) and $\gamma = 11.6 \times 10^{-3}\,\mathrm{K\,m^{-1}}$ (Juang *et al.*, 2007), the temporal variations of δ can be predicted from the time series of measured sensible heat flux collected near the surface, after imposing an initial condition on δ at some time t_0. This initial condition $\delta(t_0)$ for the slab model is given by the nocturnal equilibrium formulation in Zilitinkevich (1972), i.e.

$$\delta(t_0) = 0.4 \left(\frac{\langle \overline{u_*} \rangle}{f} \langle |L| \rangle \right)^{1/2}, \qquad \text{(A2)}$$

where the angled brackets represent the night-time average of a quantity and $f \approx 10^{-4}\,\mathrm{s^{-1}}$ is the Coriolis parameter. Time series of the average values of u_*, $\overline{T}_P$ and $\overline{w' T'_P}$ for each 27.3 min block of data from AHATS were used as input for this slab model. Data from 12 separate days of the AHATS experiment that were free from bad or missing daytime blocks in the variables of interest were used. The predicted time evolution of δ from the slab model for each day, together with the ensemble mean, can be found in Figure A1. The morning and afternoon periods are denoted with dashed vertical lines.

References

Alfredsson PH, Segalini A, Örlü R. 2011. A new scaling for the streamwise turbulence intensity in wall-bounded turbulent flows and what it tells us about the outer peak. *Phys. Fluids* **23**: 041702.

Antonia R, Raupach M. 1993. Spectral scaling in a high Reynolds number laboratory boundary layer. *Boundary Layer Meteorol.* **65**: 289–306.

Banerjee T, Katul G. 2013. Logarithmic scaling in the longitudinal velocity variance explained by a spectral budget. *Phys. Fluids* **25**: 125.

Bradshaw P. 1967. Inactive motion and pressure fluctuations in turbulent boundary layers. *J. Fluid Mech.* **30**: 241–258.

Bradshaw P. 1978. Comments on horizontal velocity spectra in an unstable surface layer. *J. Atmos. Sci.* **35**: 1768–1770.

Bremhorst K, Bullock K. 1970. Spectral measurements of temperature and longitudinal velocity fluctuations in fully developed pipe flow. *Int. J. Heat Mass Transfer* **13**: 1313–1329.

Bremhorst K, Walker T. 1973. Spectral measurements of turbulent momentum transfer in fully developed pipe flow. *J. Fluid Mech.* **61**: 173–186.

Brutsaert W. 1982. *Evaporation into the Atmosphere: Theory, History, and Applications*, Environmental Fluid Mechanics. Kluwer Academic Publishers: Dordrecht, Netherlands.

Bullock K, Cooper R, Abernathy F. 1978. Structural similarity in radial correlations and spectra of longitudinal velocity fluctuations in pipe flow. *J. Fluid Mech.* **88**: 585–608.

Businger JA, Yaglom AM. 1971. Introduction to Obukhov's paper on turbulence in an atmosphere with a non-uniform temperature. *Boundary Layer Meteorol.* **2**: 3–6.

Cai X, Peng G, Guo X, Leclerc M. 2008. Evaluation of backward and forward Lagrangian footprint models in the surface layer. *Theor. Appl. Climatol.* **93**: 207–223.

Calaf M, Hultmark M, Oldroyd H, Simeonov V, Parlange M. 2013. Coherent structures and the k^{-1} spectral behaviour. *Phys. Fluids* **25**: 125107.

Cava D, Katul GG. 2012. On the scaling laws of the velocity-scalar cospectra in the canopy sublayer above tall forests. *Boundary Layer Meteorol.* **145**: 351–367.

Charuchittipan D, Wilson J. 2009. Turbulent kinetic energy dissipation in the surface layer. *Boundary Layer Meteorol.* **132**: 193–204.

Corrsin S. 1951. On the spectrum of isotropic temperature fluctuations in an isotropic turbulence. *J. Appl. Phys.* **22**: 469–473.

Dyer A. 1974. A review of flux-profile relationships. *Boundary Layer Meteorol.* **7**: 363–372.

Erm L, Joubert P. 1991. Low-Reynolds-number turbulent boundary layers. *J. Fluid Mech.* **230**: 1–44.

Erm L, Smits A, Joubert P. 1987. Low Reynolds number turbulent boundary layers on a smooth flat surface in a zero pressure gradient. In *Turbulent Shear Flows 5*, Durst F, Launder B, Lumley J, Schmidt F, Whitelaw J. (eds.): 186–196. Springer: Berlin.

Hansen KS, Barthelmie RJ, Jensen LE, Sommer A. 2012. The impact of turbulence intensity and atmospheric stability on power deficits due to wind turbine wakes at Horns Rev wind farm. *Wind Energy* **15**: 183–196.

Heisenberg W. 1948. On the theory of statistical and isotropic turbulence. *Proc. R. Soc. London A: Math. Phys. Sci.* **195**: 402–406.

Hicks BB. 1981. An examination of turbulence statistics in the surface boundary layer. *Boundary Layer Meteorol.* **21**: 389–402.

Hinze J. 1959. *Turbulence*. McGraw-Hill: New York, NY.

Högström U. 1988. Non-dimensional wind and temperature profiles in the atmospheric surface layer: A re-evaluation. *Boundary Layer Meteorol.* **42**: 55–78.

Hsieh CI, Katul GG. 1997. Dissipation methods, Taylor's hypothesis, and stability correction functions in the atmospheric surface layer. *J. Geophys. Res.: Atmos.* **102**: 16 391--16 405.

Hsieh CI, Katul GG. 2009. The Lagrangian stochastic model for estimating footprint and water vapor fluxes over inhomogeneous surfaces. *Int. J. Biometeorol.* **53**: 87–100.

Hunt I, Joubert P. 1979. Effects of small streamline curvature on turbulent duct flow. *J. Fluid Mech.* **91**: 633–659.

Ishihara T, Yoshida K, Kaneda Y. 2002. Anisotropic velocity correlation spectrum at small scales in a homogeneous turbulent shear flow. *Phys. Rev. Lett.* **88**: 154501.

Jimenez J. 1999. The physics of wall turbulence. *Physica A* **263**: 252–262.

Juang JY, Porporato A, Stoy PC, Siqueira MS, Oishi AC, Detto M, Kim HS, Katul GG. 2007. Hydrologic and atmospheric controls on initiation of convective precipitation events. *Water Resour. Res.* **43**: W03 421.

Kader BA, Yaglom AM. 1984. *Turbulent structure of an unstable atmospheric layer, Nonlinear and Turbulent Processes in Physics*, vol. 2, Sagdeyev RZ (ed.): 829–845. Harwood Academic: Boston, MA.

Kader B, Yaglom A. 1990. Mean fields and fluctuation moments in unstably stratified turbulent boundary layers. *J. Fluid Mech.* **212**: 637–662.

Kader B, Yaglom A. 1991. Spectra and correlation functions of surface layer atmospheric turbulence in unstable thermal stratification, Turbulence and Coherent Structures, Metzds O, Lesieur M (eds.). Kluwer Academic Press: Norwell, MA, 450 pp.

Kaimal J. 1978. Horizontal velocity spectra in an unstable surface layer. *J. Atmos. Sci.* **35**: 18–24.

Kaimal JC, Finnigan JJ. 1994. *Atmospheric Boundary Layer Flows: Their Structure and Measurement*. Oxford University Press: Oxford, UK.

Katul G, Chu CR. 1998. A theoretical and experimental investigation of energy-containing scales in the dynamic sublayer of boundary-layer flows. *Boundary Layer Meteorol.* **86**: 279–312.

Katul GG, Albertson JD, Hsieh CI, Conklin PS, Sigmon JT, Parlange MB, Knoerr KR. 1996. The inactive eddy motion and the large-scale turbulent pressure fluctuations in the dynamic sublayer. *J. Atmos. Sci.* **53**: 2512–2524.

Katul G, Koning A, Porporato A. 2011. Mean velocity profile in a sheared and thermally stratified atmospheric boundary layer. *Phys. Rev. Lett.* **107**: 268502.

Katul GG, Porporato A, Nikora V. 2012. Existence of k^{-1} power-law scaling in the equilibrium regions of wall-bounded turbulence explained by Heisenberg's eddy viscosity. *Phys. Rev. E* **86**: 066311.

Katul GG, Li D, Chamecki M, Bou-Zeid E. 2013a. Mean scalar concentration profile in a sheared and thermally stratified atmospheric surface layer *Phys. Rev. E* **87**: 023004.

Katul GG, Porporato A, Manes C, Meneveau C. 2013b. Co-spectrum and mean velocity in turbulent boundary layers. *Phys. Fluids* **25**: 091 702.

Katul GG, Porporato A, Shah S, Bou-Zeid E. 2014. Two phenomenological constants explain similarity laws in stably stratified turbulence. *Phys. Rev. E* **89**: 023007.

Kim C, Entekhabi D. 1998. Feedbacks in the land-surface and mixed-layer energy budgets. *Boundary Layer Meteorol.* **88**: 1–21.

Klebanoff P. 1954. *Characteristics of Turbulence in a Boundary Layer with Zero Pressure Gradient*. NACA Technical Note 3178, National Advisory Committee for Aeronautics: Washington, DC, 1135–1153.

Kolmogorov AN. 1941. The local structure of turbulence in incompressible viscous fluid for very large Reynolds numbers. *Dokl. Akad. Nauk SSSR* **30**: 299–303.

Korotkov B. 1976. Some types of local self-similarity of the velocity field of wall turbulent flows. *Izv. Akad. Nauk SSSR Ser. Mekh. Zhidk. I. Gaza* **6**: 35–42.

Lee X, Massman W, Law BE. 2004. *Handbook of Micrometeorology: A Guide for Surface Flux Measurement and Analysis*, Vol. 29. Kluwer Academic Publihers: Dordrecht, Netherlands.

Li D, Katul GG, Bou-Zeid E. 2012. Mean velocity and temperature profiles in a sheared diabatic turbulent boundary layer. *Phys. Fluids* **24**: 105105.

Liu L, Hu F, Cheng XL. 2011. Probability density functions of turbulent velocity and temperature fluctuations in the unstable atmospheric surface layer. *J. Geophys. Res.: Atmos.* **116**: D12117.

Lumley J. 1967. Similarity and the turbulent energy spectrum. *Phys. Fluids* **10**: 855.

Lumley J, Panofsky H. 1964. *The Structure of Atmospheric Turbulence*. John Wiley and Sons: New York, NY.

McBean G. 1971. The variations of the statistics of wind, temperature and humidity fluctuations with stability. *Boundary Layer Meteorol.* **1**: 438–457.

McKeon B. 2013. Natural logarithms. *J. Fluid Mech.* **718**: 1–4.

Marusic I, Monty JP, Hultmark M, Smits AJ. 2013. On the logarithmic region in wall turbulence. *J. Fluid Mech.* **716**: R3.

Monin A, Obukhov A. 1954. Basic laws of turbulent mixing in the ground layer of the atmosphere. *Akad. Nauk. SSSR Geofiz. Inst. Trudy* **151**: 163–187.

Morrison J, Jiang W, McKeon B, Smits A. 2002. Reynolds number dependence of streamwise velocity spectra in turbulent pipe flow. *Phys. Rev. Lett.* **88**: 214501.

Nickels T, Marusic I, Hafez S, Chong M. 2005. Evidence of the k^{-1} law in a high-Reynolds-number turbulent boundary layer. *Phys. Rev. Lett.* **95**: 074501.

Nikora V. 1999. Origin of the -1 spectral law in wall-bounded turbulence. *Phys. Rev. Lett.* **83**: 734–736.

Obukhov A. 1946. Turbulence in thermally inhomogeneous atmosphere. *Trudy Inta Teoret. Geofiz. Akad. Nauk. SSSR* **1**: 95–115.

Pahlow M, Parlange MB, Porté-Agel F. 2001. On Monin–Obukhov similarity in the stable atmospheric boundary layer. *Boundary Layer Meteorol.* **99**: 225–248.

Panchev S. 1971. *Random Functions and Turbulence*. Pergamon Press: Oxford, UK.

Panofsky H, Dutton J. 1984. *Atmospheric Turbulence: Models and Methods for Engineering Applications*. John Wiley and Sons: New York, NY.

Panofsky H, Tennekes H, Lenschow DH, Wyngaard J. 1977. The characteristics of turbulent velocity components in the surface layer under convective conditions. *Boundary Layer Meteorol.* **11**: 355–361.

Perry A, Abell C. 1975. Scaling laws for pipe-flow turbulence. *J. Fluid Mech.* **67**: 257–272.

Perry A, Abell C. 1977. Asymptotic similarity of turbulence structures in smooth-and rough-walled pipes. *J. Fluid Mech.* **79**: 785–799.

Perry A, Li J. 1990. Experimental support for the attached-eddy hypothesis in zero-pressure-gradient turbulent boundary layers. *J. Fluid Mech.* **218**: 405–438.

Perry A, Henbest S, Chong M. 1986. A theoretical and experimental study of wall turbulence. *J. Fluid Mech.* **165**: 163–199.

Perry A, Lim K, Henbest S. 1987. An experimental study of the turbulence structure in smooth- and rough-wall boundary layers. *J. Fluid Mech.* **177**: 437–466.

Poggi D, Katul G, Albertson J. 2006. Scalar dispersion within a model canopy: Measurements and three-dimensional Lagrangian models. *Adv. Water Resour.* **29**: 326–335.

Pond S, Smith S, Hamblin P, Burling R. 1966. Spectra of velocity and temperature fluctuations in the atmospheric boundary layer over the sea. *J. Atmos. Sci.* **23**: 376–386.

Pope S. 2000. *Turbulence Flows*. Cambridge University Press: Cambridge, UK.

Rodean HC. 1996. Stochastic Lagrangian models of turbulent diffusion. *Meteorol. Monogr.* **26**: 1–84.

Saddoughi S, Veeravalli S. 1994. Local isotropy in turbulent boundary layers at high Reynolds number. *J. Fluid Mech.* **268**: 333–372.

Salesky S, Chamecki M. 2012. Random errors in turbulence measurements in the atmospheric surface layer: Implications for Monin–Obukhov similarity theory. *J. Atmos. Sci.* **69**: 3700–3714.

Salesky ST, Katul GG, Chamecki M. 2013. Buoyancy effects on the integral lengthscales and mean velocity profile in atmospheric surface layer flows. *Phys. Fluids* **25**: 105101.

Schumann U. 1994. On the relations between constants in homogeneous turbulence models and Heisenberg's spectral model. *Beitr. Phys. Atmos.* **67**: 141–147.

Smits AJ, Marusic I. 2013. Wall-bounded turbulence. *Phys. Today* **66**: 25–30.

Sorbjan Z. 1989. *Structure of the Atmospheric Boundary Layer*. Prentice Hall: Englewood Cliffs, NJ.

Taylor GI. 1938. The spectrum of turbulence. *Proc. R. Soc. London A: Math. Phys. Sci.* **164**: 476–490.

Tchen C. 1953. On the spectrum of energy in turbulent shear flow. *J. Res. Nat. Bur. Stand.* **50**: 51–62.

Tchen CM. 1954. Transport processes as foundations of the Heisenberg and Obukhoff theories of turbulence. *Phys. Rev.* **93**: 4.

Tennekes H. 1973. A model for the dynamics of the inversion above a convective boundary layer. *J. Atmos. Sci.* **30**: 558–567.

Townsend A. 1961. Equilibrium layers and wall turbulence. *J. Fluid Mech.* **11**: 97–120.

Townsend AA. 1976. *The Structure of Turbulent Shear Flow*. Cambridge University Press: Cambridge, UK, 428 pp.

Turan A, Azad R, Kassab S. 1987. Experimental and theoretical evaluation of the k^{-1} spectral law. *Phys. Fluids* **30**: 3463–3474.

Vickers D, Mahrt L. 1997. Quality control and flux sampling problems for tower and aircraft data. *J. Atmos. Oceanic Technol.* **14**: 512–526.

Wilson J. 2008. Monin–Obukhov functions for standard deviations of velocity. *Boundary Layer Meteorol.* **129**: 353–369.

Yaglom A. 1994. Fluctuation spectra and variances in convective turbulent boundary layers: A reevaluation of old models. *Phys. Fluids* **6**: 962.

Yang D, Meneveau C, Shen L. 2014. Large-eddy simulation of offshore wind farm. *Phys. Fluids* **26**: 025101.

Zilitinkevich S. 1972. On the determination of the height of the Ekman boundary layer. *Boundary Layer Meteorol.* **3**: 141–145.

